JMEPEG (2018) 27:3877–3885
https://doi.org/10.1007/s11665-018-3347-1

1059-9495/$19.00

High Chromium Cast Irons: Destabilized-Subcritical Secondary Carbide Precipitation and Its Effect on Hardness and Wear Properties

María Agustina Guitar, Sebastián Suárez, Orlando Prat, Martín Duarte Guigou, Valentina Gari, Gastón Pereira, and Frank Mücklich

(Submitted June 26, 2017; in revised form February 13, 2018; published online May 14, 2018)

This work evaluates the effect of a destabilization treatment combined with a subcritical diffusion (SCD) and a subsequent quenching (Q) steps on precipitation of secondary carbides and their influence on the wear properties of HCCI (16%Cr). The destabilization of the austenite at high temperature leads to a final microstructure composed of eutectic and secondary carbides, with an M_7C_3 nature, embedded in a martensitic matrix. An improved wear resistance was observed in the SCD + Q samples in comparison with the Q one, which was attributed to the size of secondary carbides.

Keywords high chromium white cast iron, microstructure, secondary carbides precipitation, solid-state transformation, wear

1. Introduction

High chromium cast irons (HCCI) have been a material of choice for wear-resistant components in the mining and mineral processing industries for a long time, given their outstanding wear and erosion resistance (Ref 1). The main reason for such resistance can be found in the hard M_nC_m reinforcement carbides embedded within the metallic matrix, being those of hypoeutectic, eutectic, or hypereutectic origin (Ref 2, 3). Hypoeutectic compositions are the main group of materials in use in the industry, with compositions described in the ASTM standard A532 groups II and III (Ref 4). Although hypereutectic HCCI would show a higher carbide volume fraction than hypoeutectic HCCI and it could be considered as a much more efficient wear-resistant material, their low castability severely hinders their practical manufacture and use (Ref 5).

The microstructure and mechanical properties of HCCI are a direct consequence of the eutectic carbide content, matrix microstructure, and the presence of secondary carbides embedded within the metallic matrix (Ref 6). Particularly, the presence of secondary carbides has shown to improve the wear resistance behavior of the entire composite (Ref 2). Secondary and also eutectic carbides characteristics are strongly influenced by the content of its main constituents (C, Cr) (Ref 2, 3, 7), minor alloying elements (Mo, Ti, V, Nb, W) (Ref 8-12), and thermal processing (Ref 5, 13).

The wear resistance and mechanical properties, especially the hardness, of HCCI depend on the type, morphology, and distribution of carbides, and on the nature of the supporting matrix structure which, in turn, depends on the chemical composition and on any subsequent thermal treatments (Ref 14-16). The secondary carbides may increase the wear resistance of the matrix itself, providing load support and reducing damage by third bodies scratching the surface, by the same mechanisms that have been studied carefully with more conventional, low reinforcement volume fraction, composite materials (Ref 17, 18). To some extent, the precipitation of secondary carbides should lead to a more bimodal-like reinforced composite behavior, which has been proved previously to have a better wear performance than its mono-modal counterparts (Ref 19, 20).

Besides, the secondary carbides which precipitate in the matrix regions also influence wear resistance by increasing the matrix strength through dispersion strengthening and microstructure refinement, and the fine secondary carbides can increase the mechanical support of the eutectic carbides (Ref 10, 11, 21).

Precipitation of secondary carbides during a subcritical destabilization treatment (Ref 22) has been previously described for HCCI and the usual quenching procedure, i.e., holding temperatures above the critical line (from 0.5 to 4 h) before cooling in air. In most cases, the authors compared the latter to a series of subcritical approaches as references (Ref 11, 23, 24). Heat treatments are designed to precipitate a fine dispersion of Fe-Cr carbides within the matrix. Multi-step treatments have been proposed (martensite formation and post-quench subcritical annealing for carbide precipitation), with a significant secondary carbide precipitation, although the intermediate air cooling induced a sharp decrease in mechanical properties. The decrease in mechanical properties was associated with the formation of ferrite phases in the subcritical step; in general, subcritical treatments have been associated with

María Agustina Guitar, Sebastián Suárez, and **Frank Mücklich**, Department of Materials Science, Saarland University, Campus D3.3, 66123 Saarbrücken, Germany; **Orlando Prat**, Departamento de Ingeniería de Materiales, Universidad de Concepción, Edmundo Larenas 270, Concepción, Chile; **Martín Duarte Guigou**, Programa de Ingeniería de Materiales, Facultad de Ingeniería y Tecnologías, Universidad Católica del Uruguay, Av. 8 de Octubre 2738, CP 11600 Montevideo, Uruguay; and Laboratorio de Desarrollo de Nuevos Materiales, Tubacero S.A., Cnel. Raíz 949, CP 12900 Montevideo, Uruguay; **Valentina Gari**, Programa de Ingeniería de Materiales, Facultad de Ingeniería y Tecnologías, Universidad Católica del Uruguay, Av. 8 de Octubre 2738, CP 11600 Montevideo, Uruguay; and **Gastón Pereira**, Laboratorio de Desarrollo de Nuevos Materiales, Tubacero S.A., Cnel. Raíz 949, CP 12900 Montevideo, Uruguay. Contact e-mail: a.guitar@mx.uni-saarland.de.

hardness reduction (Ref 25). Furthermore, the type, size, and distribution of secondary carbides formed during the destabilization depend on the composition and destabilization temperature. The secondary carbides are efficient for improving the abrasion resistance (Ref 26, 27).

The proposed destabilized plus subcritical diffusion treatment should lead to a sharper increase in size and a better distribution of secondary carbides within the matrix, without affecting other mechanical properties. Assuming that this material behaves tribologically as a bimodal size reinforced MMC, the post-treatment wear resistance should improve, despite the slight changes in other mechanical properties (Ref 23, 28).

In this work, contrary to other works found in the literature (Ref 25), a destabilization process is carried out followed directly by a subcritical diffusion (SCD) step in order to precipitate and grow secondary carbides. The main objectives of the present work are: (a) to analyze whether increased secondary carbide precipitation is achievable with a high-temperature destabilization and multi-step subcritical heat treatment, using limited minor alloying elements and preserving mechanical properties; (b) to compare such results with a standard above critical destabilization treatment, and (c) to analyze the effect of such increased carbide precipitation on wear resistance.

2. Experimental

HCCI samples were manufactured in arc furnace and cast in cubic sand molds. Chemical composition was determined by emission spectroscopy methods using a GNR Metal Lab 75/80 Optical Emission Spectroscope. The chemical composition of the studied HCCI is: C (2.43 wt.%)-Si (0.47 wt.%)-Mn (0.76 wt.%)-Cr (15.84 wt.%)-Ni (0.41 wt.%)-S (0.02 wt.%)-P (0.02 wt.%)-Cu (0.04 wt.%)-Fe (balance).

The thermal treatments were carried out by two methods: (1) destabilization above critical temperature (1253 K) and quenching and (2) destabilization followed by a subcritical diffusion (SCD) process at 923 K for 12 h. Destabilization temperature was determined as critical temperatures plus 50 K, and SCD temperature was set at 50 K below zero transformation temperature for the corresponding chemical composition for maximum carbide precipitation. Thus, observations were carried out in four samples: (1) as-cast conditions, (2) SCD, (3) quenched (Q), and (4) SCD + Q, being the SCD sample an intermediate state. Schematic representation for each treatment is shown in Fig. 1.

The samples were ground with embedded diamond discs (up to grit 1200) and polished using diamond powder suspensions up to 1 μm mean diameter. The samples were etched with Vilella's reagent (1 g picric acid + 5 mL HCl 100 mL ethanol) for 30 s at room temperature. Optical microscopy observations were carried out in all samples using a Leica CTR6000 microscope, and images were acquired using a Jenoptik CCD Camera.

SEM characterization was carried out with a FE-SEM Helios Nanolab 600 (FEI company) working with an acceleration voltage of 10 kV and a 1.4 nA beam current. For a proper contrast between phases, a high-sensitivity solid-state backscattered electrons detector (vCD) was used. Electron backscattered diffraction with an acceleration voltage of 20 kV and 11 nA

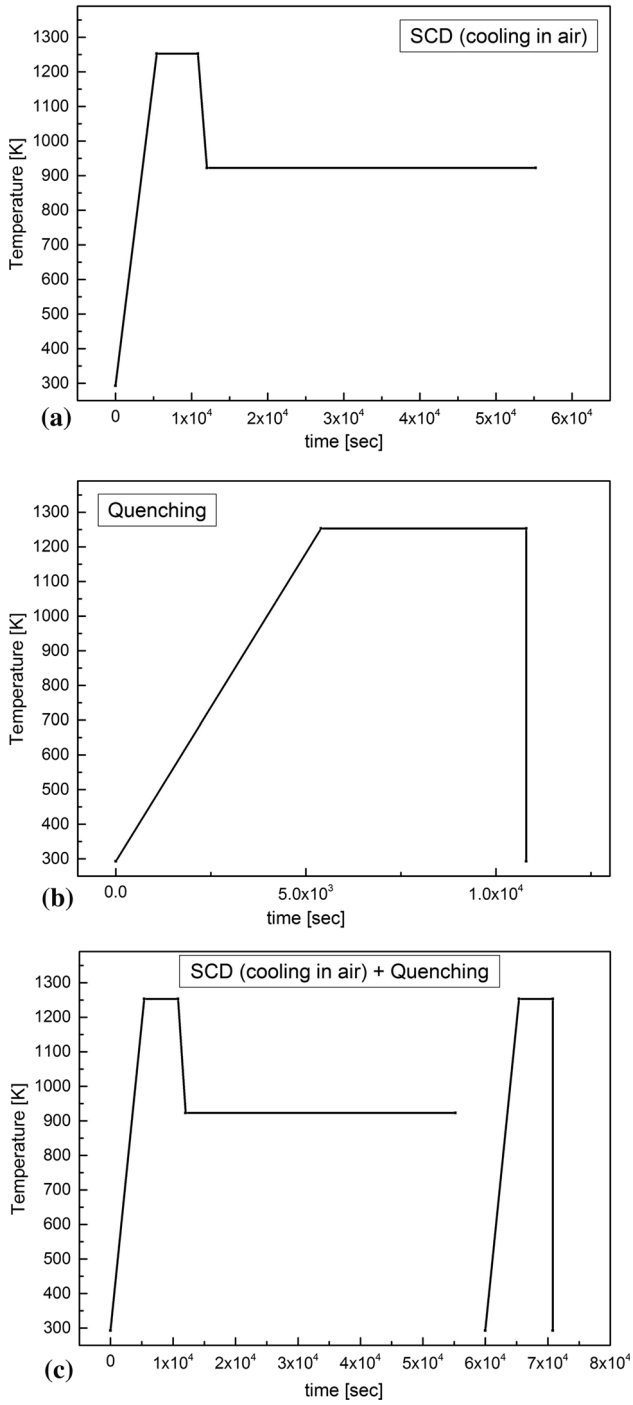

Fig. 1 Schematic representation for the different thermal treatments (a) quenching, (b) subcritical diffusion, and (c) subcritical diffusion followed by quenching

beam current together with the TSL OIM Data Collection software was used for the carbide type identification.

Macrohardness on the Rockwell C scale was measured using a Wilson durometer with a diamond indenter and 150 Kgf load. Microhardness was measured with a Leica Vickers microindenter applying 0.500 Kgf load on all samples for both matrix and primary carbides. The indentation time in all cases was 15 s.

X-ray diffraction testing was performed with a PANalytical Empyrean x-ray diffractometer. The diffractograms were

obtained using a symmetrical θ–θ geometry configuration and a Cu Kα_1 radiation ($\lambda = 0.15406$ nm). The incident and diffracted optical geometries were parallel, and the diffraction angle (2θ) was varied from 25° to 100° with a step size of 0.013° and a 50 s/step rate. The applied voltage and current were 40 kV and 40 mA, respectively. For the phase identification and indexing, the High Score Plus software and ICDD Database were used.

Wear test was carried out in a CSM macro-tribometer in rotational mode using an alumina pin, applying a 5 N load for 4000 laps with 2.46 mm radius at a speed of 5.0 cm/s with environment conditions set at 298 K (25 °C) and 45% humidity. Wear tracks were observed using a Zygo NewView 7300 white light interferometer (for wear volume calculations) and SEM microscopy.

3. Results and Discussion

3.1 Phase and Microstructural Evolution

Figure 2 shows the XRD measurements for the different states of the treated samples. The as-cast condition is represented by the eutectic carbide embedded in an austenitic matrix (M_7C_3/Fe-γ), as described in (Ref 25) and also predicted in the Jackson's diagram for the Fe-Cr-C system (Ref 29). Some authors also reported the presence of martensite surrounding the eutectic carbide particles as a result of the excessive consumption of C and Cr by the eutectic carbides (Ref 25). Consequently, the matrix remains depleted in these elements, resulting in the increase of the *Ms* temperature and promoting the martensite formation.

The SCD treatment leads to the transformation of the matrix from austenite to ferrite, and carbides of the form M_7C_3 were detected. XRD measurements confirm the absence of martensite in this sample, whose presence is not expected since the sample was cooled in air after the subcritical diffusion treatment. On other way, the quenching of the material (Q sample) generates a complete martensitic transformation of the matrix. Very small peaks corresponding to M_7C_3 are also observed. The SCD + Q sample showed, just like the Q sample, a matrix formed by martensite and carbides of the form M_7C_3. In the inset of Fig. 2, the most intense peaks from ferrite and martensite are shown. A shift in the diffraction angle and an increasing width of the peak, as a consequence of the lattice distortion, allow the identification of martensite-form ferrite.

In order to corroborate the obtained phases in the Q and SCD + Q samples, thermodynamic calculations with the Thermo-Calc software and EBSD measurements were performed, see Fig. 3. The simulation was performed using all the elements of the studied alloy, and using the TCFe8 database. Figure 3(a) shows the fraction of the stable phases in the system at different temperatures. From the thermodynamic point of view, it is possible to state that the only stable precipitate within the performed heat treatment temperature range in the alloy is of the type M_7C_3, validating the results obtained by XRD. Moreover, EBSD was used for the characterization of individual secondary carbides (about 40 secondary carbides were randomly measured). In all cases, a hexagonal crystallographic structure was detected, which corresponds to the M_7C_3 carbides (Fig. 3b). The precipitation of $M_{23}C_6$-type carbides might only be possible at temperatures under 738 K (465 °C), whereas cementite (M_3C) is not expected to precipitate due to the high amount of Cr. Furthermore, it is well known that carbide-forming elements replace the less stable cementite, which dissolves into a finer alloy carbide dispersion (Ref 21). This replacement by the alloy carbides, which is more resistant to coarsening, is able to produce an increase in hardness at higher temperatures (Ref 21). The strengthening efficiency of this carbide dispersion will depend on the refinement of the precipitates and their volume fraction.

Figure 4 shows the microstructure for the as cast, SCD, Q, and SCD + Q samples. The as-cast microstructure is composed of primary austenite matrix surrounded by the eutectic mixture

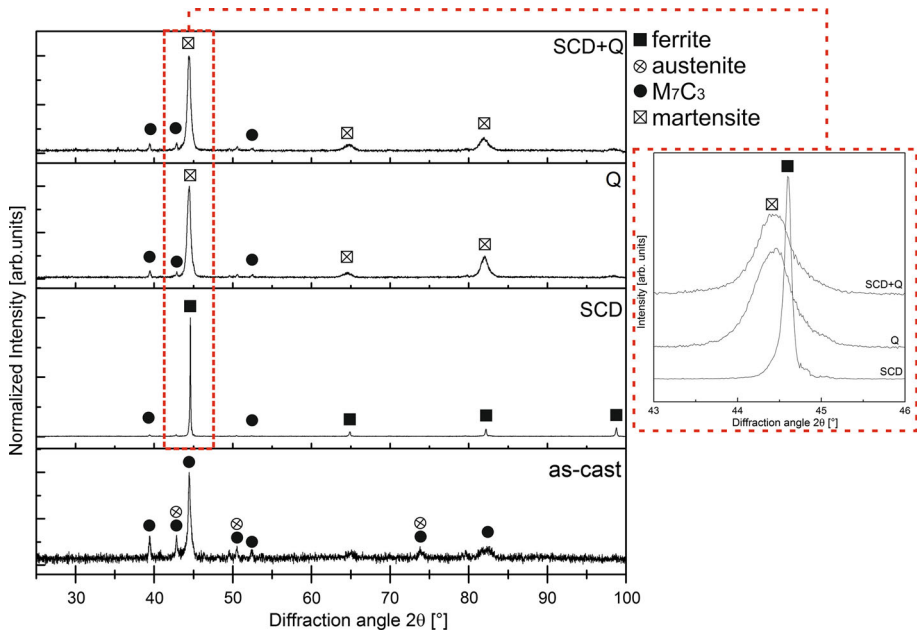

Fig. 2 XRD diffractograms for the different thermal treatments. The inset in the image shows the shift and peak width of the martensite diffraction peaks (samples Q and SCD + Q) with respect to those from the ferrite (sample SCD)

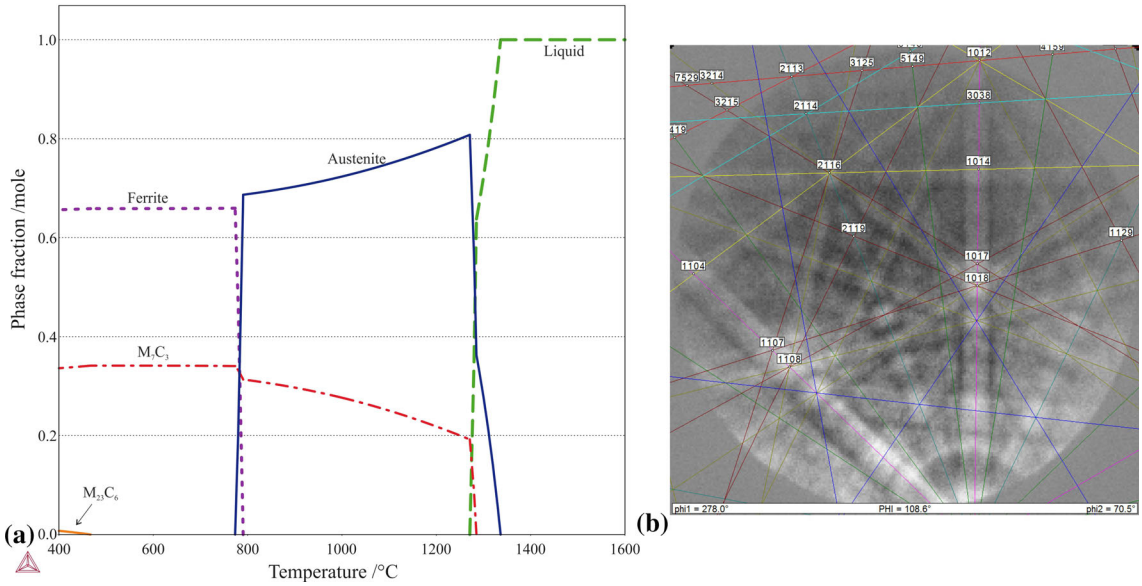

Fig. 3 (a) Phase fraction vs. temperature diagram, calculated with thermocalc and (b) Kikuchi patterns corresponding to the secondary carbides showing the hexagonal crystallographic structure (M_7C_3 type)

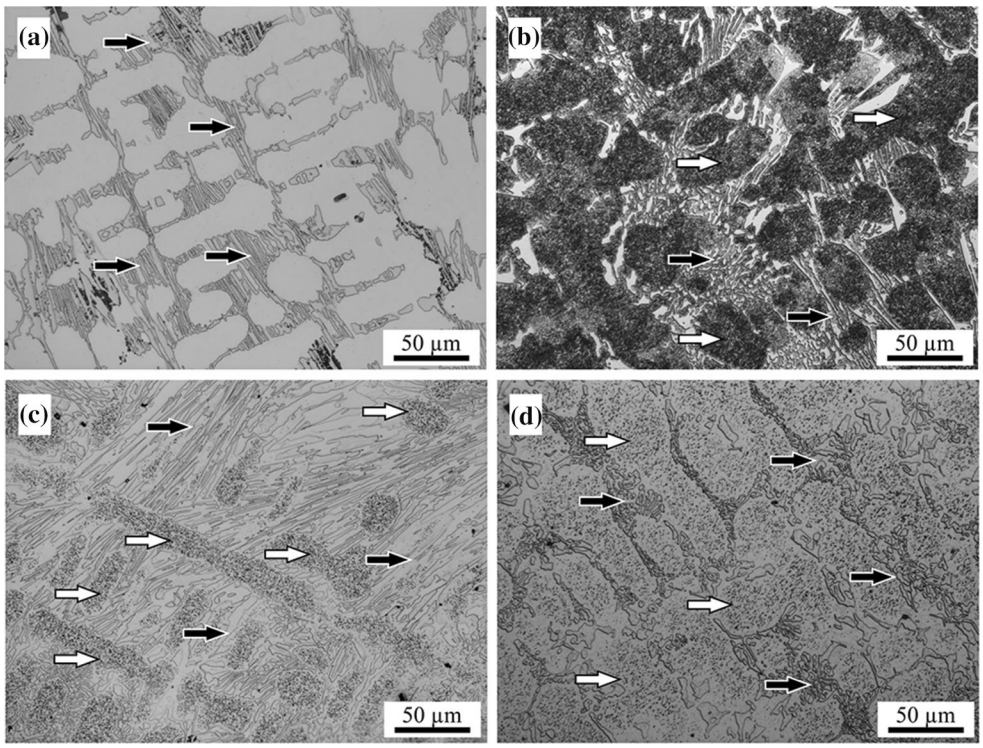

Fig. 4 Optical microscopy images showing: (a) the as-cast condition; (b) the SCD sample; (c) the Q sample; and (d) the SCD + Q sample. The samples were etched with Vilella's reagent for matrix/carbide contrast. Black arrows indicate the regions of eutectic carbides, and the white arrows indicate regions of secondary carbides

of M_7C_3 carbides/austenite, as also indicated in the diffractogram of Fig. 2. Given the Cr and C content, no secondary carbides are expected to be observed in this sample. This microstructure is the starting point for the subsequent heat treatments previously described in Fig. 1. SCD process produces a microstructure of ferrite and secondary carbides. The etching employed here (Vilella's reagent) attacks the ferrite-carbide microstructure; therefore, the optical image in Fig. 4(b) shows dark regions corresponding to this type of microstructure, which is result of the high concentration of small secondary carbides. The Q and SCD + Q microstructures (Fig. 4c, d) show a fine martensitic matrix surrounding the

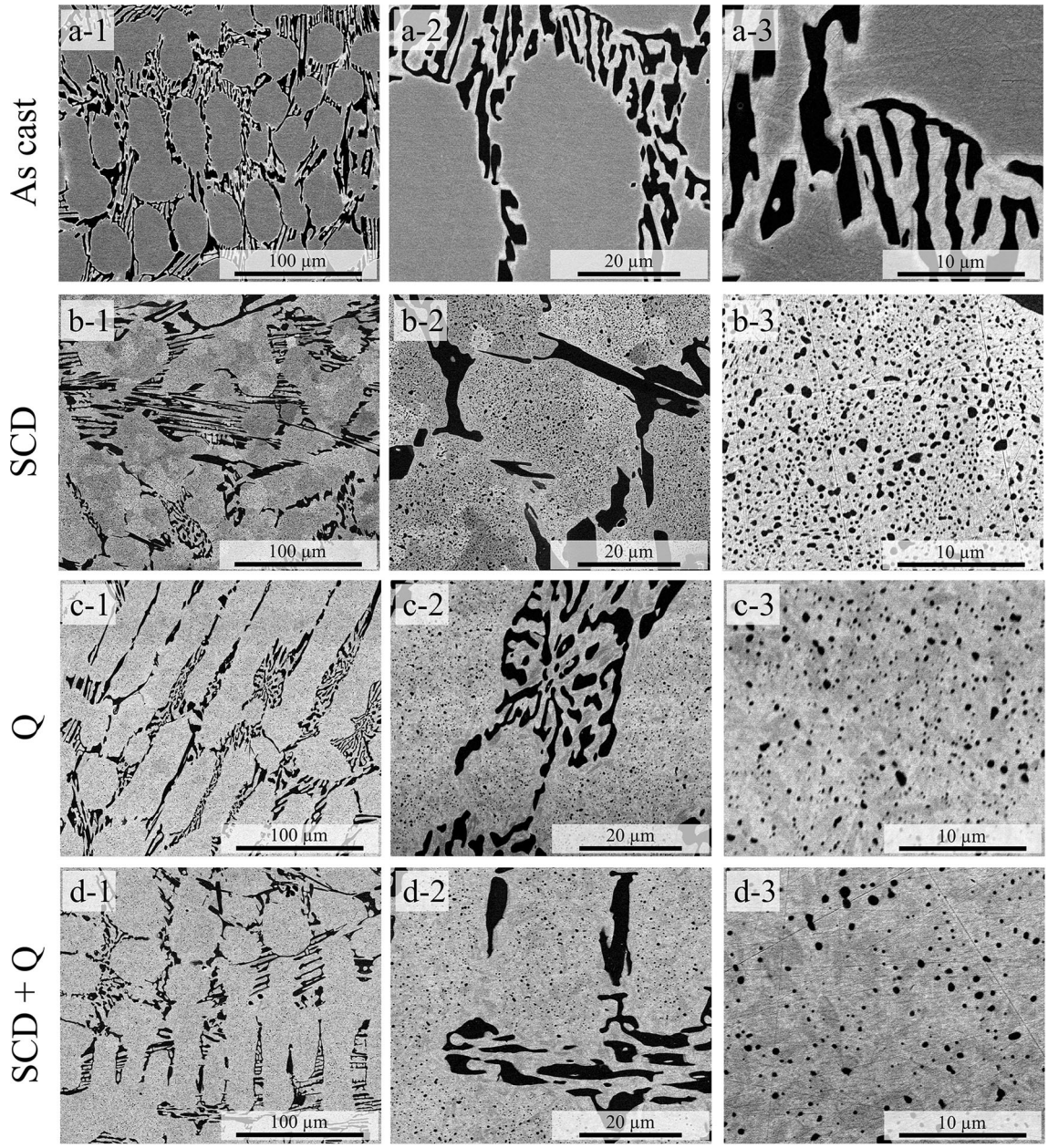

Fig. 5 SEM (BSE) images for all the samples at different magnifications from left to right × 500, × 2000 and × 6500, respectively. (a) As cast, (b) SCD, (c) Q, and (d) SCD + Q

unchanged eutectic carbide phase when compared with as-cast conditions. Small secondary carbides are expected to be present in these samples; however, they cannot be resolved with optical microscopy techniques. Black and white arrows in Fig. 4 indicate the regions of eutectic and secondary carbides, respectively. For better resolution and details of the presence and distribution of secondary carbides, SEM images were acquired (Fig. 5).

SEM images in BSE mode for all the samples taken at different scales are shown in Fig. 5. As previously described, no secondary carbides are observed in the austenitic matrix of the as-cast condition. The destabilization treatment above the critical temperature 1253 K (980 °C) allows the precipitation of secondary carbides, as shown in SCD (Fig. 5b), Q (Fig. 5c), and SCD + Q (Fig. 5d) samples. As learned from the XRD results, in the SCD sample, the secondary carbides are embedded in a ferritic matrix, whereas in the Q and SCD + Q samples, in a martensitic matrix. In all cases, the secondary carbides have apparently randomly nucleated and they show a round-like morphology.

The addition of a subcritical diffusion (SCD) process following the destabilization step caused visible modifications compared to the as-cast material and also to quenched material. Large quantities of secondary carbides were precipitated within the austenitic matrix, which have transformed completely to ferrite by holding the temperature at 923 K (650 °C) (see Fig. 2). Secondary carbides of different sizes can be observed embedded in the matrix. The prolonged duration of the SCD process allows the precipitation of a large quantity of new carbides and the growth of those precipitated during the

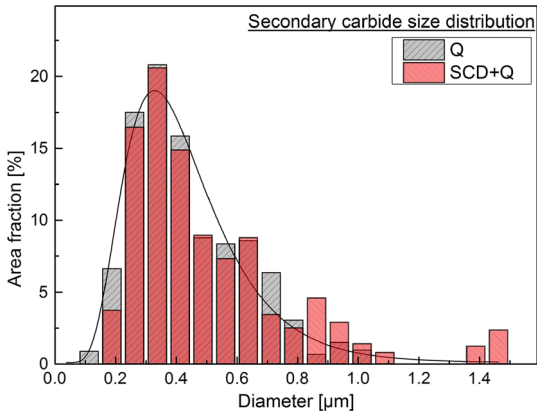

Fig. 6 Secondary carbides size distribution obtained after image analysis of SEM (BSE) images

destabilization step. This is clearly observable comparing Fig. 5(b) and (c).

The Q and SCD + Q samples do not show a noticeable change in the amount of secondary carbides. However, the SCD + Q sample (Fig. 5d) shows an apparent increase in size of secondary carbides inside the martensitic matrix (compared to the Q sample). The secondary carbides size was determined after image analysis (I-A) of SEM (BSE) micrographs using the software A4i©. The calculated average carbide size was 0.44 and 0.51 µm for the Q and SCD + Q samples, respectively. The combination of a SCD state and quenching provides a coarse-sized secondary carbide distribution throughout the matrix, as indicated in the carbide size distribution of Fig. 6 and also supported by the evidence observed by electron microscopy (Fig. 5). This results from the subcritical diffusion treatment which allows the secondary carbides to increase in size, mainly due to an extended time of energy input to the system.

3.2 Hardness and Wear Response Evaluation

It is well known that the microstructure plays a fundamental role in the resulting mechanical properties. The wear resistance and mechanical properties, especially the hardness of HCCI, depend on the type, morphology, and distribution of carbides, and on the nature of the supporting matrix structure which, in turn, depends on the chemical composition and subsequent thermal treatments (Ref 14-16). For this reason, the influence of the microstructure after thermal treatments in the wear response is being analyzed in this section.

The mechanical properties play a fundamental role in the applicability of these materials in the field. They would determine their machinability and subsequently, define the application in components. Specifically, microhardness measurements show the variations of local mechanical properties which may significantly influence the abrasion behavior of the material (Ref 30). The macro- and microhardness values of three different stages are represented in Fig. 7(a) and (b), respectively. The expected change in macrohardness due to the austenitic (as-cast sample) to martensitic (Q and SCD + Q samples) matrix change is clearly noticeable (Fig. 7a). However, the presence of secondary carbides might not be dismissed as an influencing factor for this improvement. However, when comparing the results for the Q and SCD + Q samples, no significant changes are observed, since both present the same type of matrix. Thus, it is consequential to state that the main

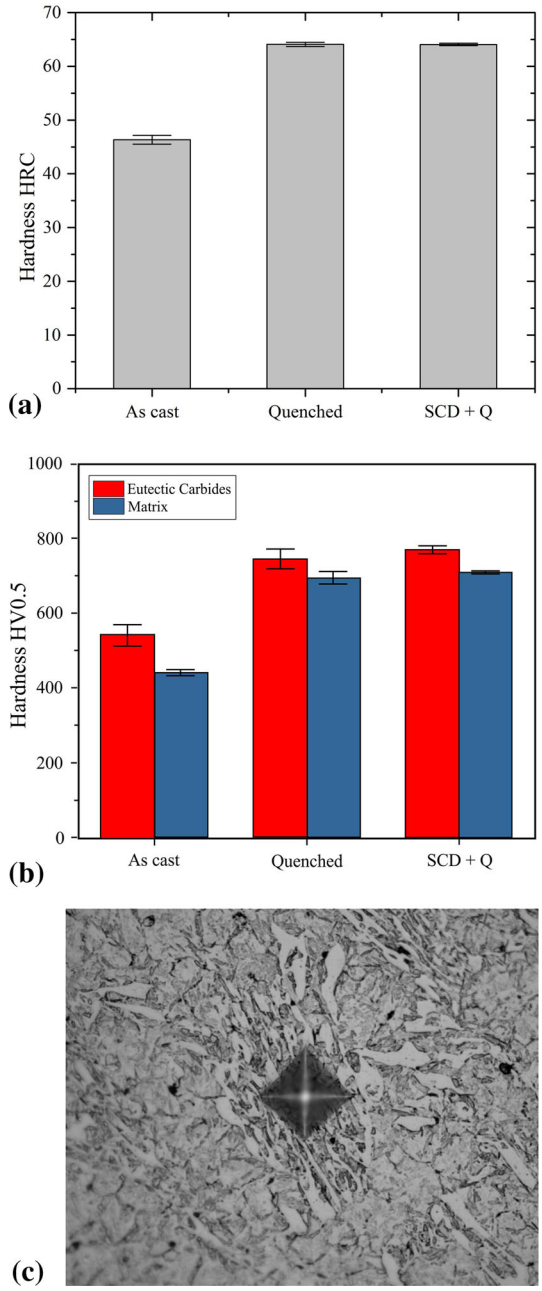

Fig. 7 (a) Hardness test results in the Rockwell C Scale and (b) microhardness measurements for three microstructural states: as cast, Q, and SCD + Q. Standard deviation of the measures is also plotted. (c) Optical micrograph showing the area influenced by the microindentation during the eutectic zone measurement

role regarding the mechanical properties is played by the matrix transformation. Microhardness measurements were performed on both the matrix and the eutectic carbides. The same trend as in the macrohardness measurements was observed when only the matrix is evaluated, as shown in Fig. 7(b). Additionally, a slight but not statistically representative increase in the matrix microhardness of the SCD + Q sample can be observed in comparison with the Q sample. However, when the eutectic carbides zone is evaluated, both the carbides' intrinsic mechanical response and the surrounding matrix behavior are considered as a whole system due to the indentation size effects (Fig. 7c). The same increase in microhardness is observable in

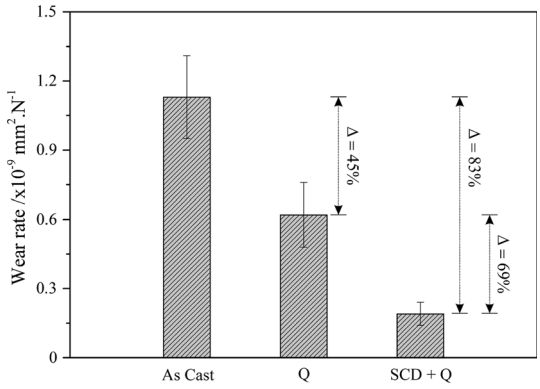

Fig. 8 Wear rate volume in $mm^2\ N^{-1}$ calculated after pin on disc test for the different treated samples

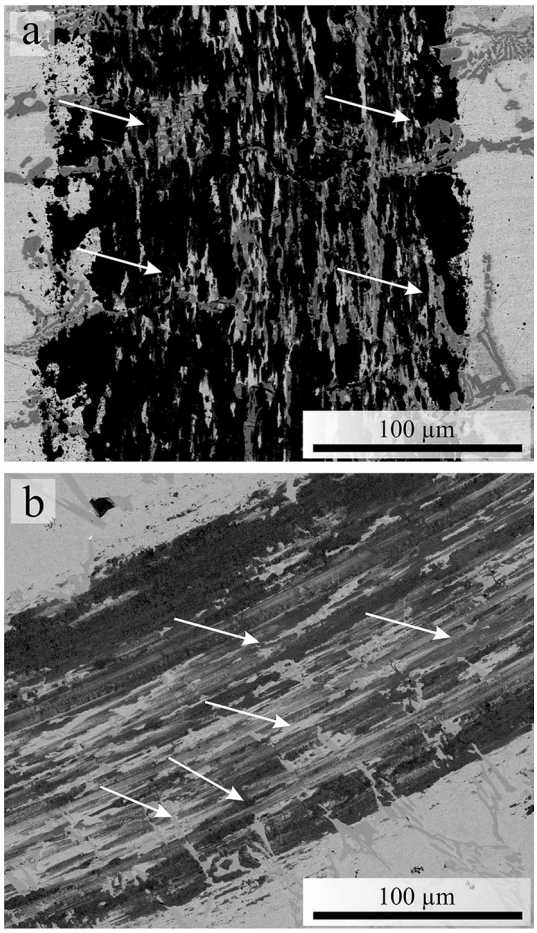

Fig. 9 (a) Backscattered electron micrograph of the wear track in the as-cast sample and (b) wear track of the quenched sample. The darker areas are tribologically induced oxides, whereas the lighter regions are either carbides or unmodified matrix material. The white arrows indicate regions where the eutectic carbides remain unworn

the eutectic carbide areas of the SCD + Q with respect to the Q sample. Those similar hardness values in Q and SCD + Q are mainly due to the precipitation of the same type of secondary carbides.

When comparing the microhardness of the eutectic carbide-containing regions of both heat-treated samples to the as-cast condition, the difference can be attributed to the increase in the supporting role of the matrix surrounding the eutectic carbides. It is worth noting that in all cases, an incoherent interface between the M_7C_3 phase and the matrix is expected, since the interatomic distances show a misfit larger than 25% (Ref 21). This would further account for an efficient particle dispersion strengthening due to the effective hindering of dislocation mobility. Additionally, it has been reported that the quenching step adds a thermal strain to the matrix, which results in a dislocation punching during plastic strain and accounts for a significant strengthening (Ref 31).

Regarding the tribological behavior of the materials, the wear rates after pin on disc tests are shown in Fig. 8. A significant reduction in wear rate of the Q and SCD + Q samples is observed when compared to the as-cast condition, being 45 and 83%, respectively. These results correlate quite well with the hypothesis that harder materials tend to show lower wear rates, given by the conventional Archard behavior/relationship (Ref 32). However, both heat-treated samples show a strongly differentiated wear behavior. Specifically, the SCD + Q sample showed a reduction of 69% compared to the quenched state.

This enhanced wear resistance of the SCD + Q sample cannot be explained by the macro- and microhardness values. It has already been reported that the wear behavior shows a weak dependency on the macrostructure (Ref 26). Thus, for the wear response of this type of materials (which should be considered as composite materials), not only the carbide structure or distribution should be considered, but also the nature of the matrix surrounding the carbides and their interaction as a whole must be taken into account. This synergistic effect is well known in multimodal systems (Ref 19). An important role in the improvement in wear response of Q and SCD + Q samples is played, as already shown for the hardness, by the austenite/martensite transformation of the matrix added to the secondary carbides precipitated on the treated samples. Furthermore, even in cases where a full martensitic transformation is not achieved, the amount of retained austenite might enhance the response by acting in two ways: inactivating the crack tip formation and hindering the crack development coming from more brittle phases (Ref 27).

During the wear test, oxidation occurs predominantly on the matrix parts of the track (Fig. 9), whereas carbides are usually very slightly affected (Ref 33). This oxidation leads to a continuous generation of hard and brittle wear particles that are consistently introduced to the sliding contact, thus inducing an oxide-driven transition from a mild to a severe third-body wear activity. Additionally, it has been reported for related systems that the wear rate decreases either with increasing carbide volume fraction (CVF) or with the increasing carbide size for the same CVF (Ref 26). In both heat-treated samples, the total CVF is expected to be the same, since they present the same chemical composition. Yet, some difference was observed in the size distribution of the secondary carbides of both samples (as observed in Fig. 6), being larger in the SCD + Q sample. Hence, these larger carbides provide an effective protection to the matrix (more wear prone) from the abrasion. Additionally, a higher crack density has been observed in carbides with the larger axis parallel to the wear surface (Ref 26), indicating a strong capacity of the carbides to absorb energy during friction. Then, it would be reasonable to expect that the sample that shows a larger mean secondary carbide size will provide larger non-reactive areas of load support (in this case, the SCD + Q sample) and would therefore present a lower wear rate.

Summarizing, this work shows that the application of a multi-step thermal treatment of a high chromium cast iron consisting of the austenite destabilization and a subsequent quenching leads to the precipitation of carbides inducing a significant reduction in the wear loss by an accurate tailoring of the secondary phase. When compared to a traditional quenching process, the same matrix phase is obtained but with different mean secondary carbide size, which further translates into better wear response without sacrificing the overall mechanical properties.

4. Concluding Remarks

In this study, we evaluated the effect of a destabilization treatment combined with a subcritical diffusion and quenching steps in the secondary carbides precipitation and their influence on the wear properties. It was observed that HCCI in the as-cast condition composed of an austenitic matrix and eutectic carbides are not sufficient for a good abrasive wear resistance. In all cases, secondary carbides precipitated within the matrix are needed for an increase in wear response. A destabilization process followed by a SCD step allows not only the precipitation but also the growth of secondary carbides. An additional destabilization and quenching stages transform the matrix into martensite, resulting in a matrix with a higher hardness but no observable changes in secondary carbides. This process sequence also avoids the presence of ferrite (or pearlite) in the final microstructure, which would be detrimental to the mechanical properties. Finally, an improved wear resistance was observed in the SCD + Q sample compared to the Q one, being the size of secondary carbides apparently responsible for this behavior. For this, the destabilization followed by a SCD is a fundamental step for the secondary carbides growth.

Wear mechanisms will be thoroughly analyzed in a further work, in order to evaluate the effect of microstructure changes in the wear rate and wear mechanisms, principally those related to the secondary carbides nature, shape, and size.

Acknowledgments

This work was supported by the CREATE Network Project, Horizon 2020 Program of the European Commission (RISE Project No. 644013). The authors want to thank Priv.-Doz. Dr. Jose Garcia from AB Sandvik Coromant R&D (Technology Area Manager Carbide and Sintering) for the helpful discussion and verification of some of the results.

References

1. R.J. Llewellyn, S.K. Yick, and K.F. Dolman, Scouring Erosion Resistance of Metallic Materials Used in Slurry Pump Service, *Wear*, 2004, **256**, p 592–599
2. X.H. Tang, R. Chung, D.Y. Li, B. Hinckley, and K. Dolman, Variations in Microstructure of High Chromium Cast Irons and Resultant Changes in Resistance to Wear, Corrosion and Corrosive Wear, *Wear*, 2009, **267**, p 116–121
3. C. Scandian, C. Boher, J.D.B. de Mello, and F. Rézaï-Aria, Effect of Molybdenum and Chromium Contents in Sliding Wear of High-Chromium White Cast Iron: The Relationship Between Microstructure and Wear, *Wear*, 2009, **267**, p 401–408
4. ASTM International, A532/A532M "Standard Specification for Abrasion-Resistant Cast Irons", ASTM International, West Conshohocken, 2003, p 1–4
5. X. Zhi, J. Xing, Y. Gao, H. Fu, J. Peng, and B. Xiao, Effect of Heat Treatment on Microstructure and Mechanical Properties of a Ti-Bearing Hypereutectic High Chromium White Cast Iron, *Mater. Sci. Eng. A*, 2008, **487**, p 171–179
6. ASM International, ed., "ASM Handbook, Volume 1: Properties and Selection: Irons, Steels, and High-Performance Alloys", 10th ed., ASM International, 1990
7. D. Li, L. Liu, Y. Zhang, C. Ye, X. Ren, Y. Yang et al., Phase Diagram Calculation of High Chromium Cast Irons and Influence of Its Chemical Composition, *Mater. Des.*, 2009, **30**, p 340–345
8. A. Bedolla-Jacuinde, R. Correa, I. Mejía, J.G. Quezada, and W.M. Rainforth, The Effect of Titanium on the Wear Behaviour of a 16%Cr White Cast Iron Under Pure Sliding, *Wear*, 2007, **263**, p 808–820
9. R.J. Chung, X. Tang, D.Y. Li, B. Hinckley, and K. Dolman, Effects of Titanium Addition on Microstructure and Wear Resistance of Hypereutectic High Chromium Cast Iron Fe-25wt.%Cr-4wt.%C, *Wear*, 2009, **267**, p 356–361
10. J. Wang, R.L. Zuo, Z.P. Sun, C. Li, H.H. Liu, H.S. Yang et al., Influence of Secondary Carbides Precipitation and Transformation on Hardening Behavior of a 15 Cr-1 Mo-1.5 v White Iron, *Mater. Charact.*, 2005, **55**, p 234–240
11. M. Filipovic, Z. Kamberovic, M. Korac, and M. Gavrilovski, Microstructure and Mechanical Properties of Fe–Cr–C–Nb White Cast Irons, *Mater. Des.*, 2013, **47**, p 41–48
12. S.H. Mousavi Anijdan, A. Bahrami, N. Varahram, and P. Davami, Effects of Tungsten on Erosion–Corrosion Behavior of High Chromium White Cast Iron, *Mater. Sci. Eng. A*, 2007, **454–455**, p 623–628
13. J. Wang, J. Xiong, H. Fan, H.-S. Yang, H.-H. Liu, and B.-L. Shen, Effects of High Temperature and Cryogenic Treatment on the Microstructure and Abrasion Resistance of a High Chromium Cast Iron, *J. Mater. Process. Technol.*, 2009, **209**, p 3236–3240
14. D. Kopyci, E. Guzik, D. Siekaniec, and A. Szcz, Analysis of the High Chromium Cast Iron Microstructure after the Heat Treatment, *Arch. Foundry Eng.*, 2014, **14**, p 43–46
15. A. Wiengmoon, J.T.H. Pearce, and T. Chairuangsri, Relationship Between Microstructure, Hardness and Corrosion Resistance in 20 wt.% Cr, 27 wt.% Cr and 36 wt.% Cr High Chromium Cast Irons, *Mater. Chem. Phys.*, 2011, **125**, p 739–748
16. S.D. Carpenter, D. Carpenter, and J.T.H. Pearce, XRD and Electron Microscope Study of an As-Cast 26.6% Chromium White Iron Microstructure, *Mater. Chem. Phys.*, 2004, **85**, p 32–40
17. M. Duarte, J. Molina, R. Prieto, E. Louis, and J. Narciso, Effects of Particle Size and Volume Fraction on Wear Behavior of Aluminum Alloys/Ceramic Particles Composites, *Solidification Processing of Metal Matrix Composite*, 2006 TMS Annual Meeting, San Antonio, TX, 2006, p 249–257
18. C. García-Cordovilla, J. Narciso, and E. Louis, Abrasive Wear Resistance of Aluminium Alloy/Ceramic Particulate Composites, *Wear*, 1996, **192**, p 170–177
19. A. Demir, N. Altinkok, F. Findik, and I. Ozsert, The Wear Behaviour of Dual Ceramic Particles (Al_2O_3/SiC) Reinforced Aluminium Matrix Composites, *Key Eng. Mater.*, 2004, **264–268**, p 1079–1082
20. S. Kumar, R.S. Panwar, and O.P. Pandey, Effect of Dual Reinforced Ceramic Particles on High Temperature Tribological Properties of Aluminum Composites, *Ceram. Int.*, 2013, **39**, p 6333–6342
21. D.A. Porter and K.E. Easterling, *Phase Transformations in Metals and Alloys*, CRC Press, Boca Raton, 1992
22. Z. Sun, R. Zuo, C. Li, B. Shen, J. Yan, and S. Huang, TEM Study on Precipitation and Transformation of Secondary Carbides in 16Cr-1Mo-1Cu White Iron Subjected to Subcritical Treatment, *Mater. Charact.*, 2004, **53**, p 403–409
23. M. Filipovic, Z. Kamberovic, M. Korac, and M. Gavrilovski, Correlation of Microstructure with the Wear Resistance and Fracture Toughness of White Cast Iron Alloys, *Met. Mater. Int.*, 2013, **19**, p 473–481
24. A. Wiengmoon, T. Chairuangsri, A. Brown, R. Brydson, D.V. Edmonds, and J.T.H. Pearce, Microstructural and Crystallographical Study of Carbides in 30wt.%Cr Cast Irons, *Acta Mater.*, 2005, **53**, p 4143–4154

25. A.E. Karantzalis, A. Lekatou, and H. Mavros, Microstructural Modifications of As-Cast High-Chromium White Iron by Heat Treatment, *J. Mater. Eng. Perform.*, 2009, **18**, p 174–181
26. Ö.N. Doğan, J.A. Hawk, and G. Laird, Solidification Structure and Abrasion Resistance of High Chromium White Irons, *Metall. Mater. Trans. A*, 1997, **28**, p 1315–1328
27. H. Gasan and F. Erturk, Effects of a Destabilization Heat Treatment on the Microstructure and Abrasive Wear Behavior of High-Chromium White Cast Iron Investigated Using Different Characterization Techniques, *Metall. Mater. Trans. A*, 2013, **44**, p 4993–5005
28. J.Q. Xu, Y.Y. Chen, W. Wang, K.P. Liu, H.S. Liu, and Y.D. Xiao, Sliding Friction Properties of Austenite-and Martensite-Based White Cast Iron Containing 8.5% Chromium, *J. Mater. Sci.*, 2010, **45**, p 6108–6114
29. J.D.B. DeMello, M. Durand-Charre, and S. Hamar-Thibault, Solidification and Solid State Transformations During Cooling of Chromium-Molybdenum White Cast Irons, *Metall. Trans. A*, 1983, **14**, p 1793–1801
30. J. Chen, M. Lv, S. Tang, Z. Liu, and G. Wang, Correlation Between Mechanical Properties and Retained Austenite Characteristics in a Low-Carbon Medium Manganese Alloyed Steel Plate, *Mater. Charact.*, 2015, **106**, p 108–111
31. K.K. Chawla, *Composite Materials: Science and Engineering*, 3rd ed., Springer, New York, 2012
32. H. Czichos and K.-H. Habig, *Tribologie Handbook*, 2nd ed., Friedr. Vieweg & Son Verlag, 2003
33. S. Atapek and S. Polat, A Study of Wear of High-chromium Cast Iron Under Dry Friction, *Met. Sci. Heat Treat.*, 2013, **55**, p 181–183